

AFRL-AFOSR-UK-TR-2015-0011



Toward ultrasonic tunable ultra-damping metamaterials

**Oliver Mondain-Monval, O. Sandre, T. Brunet, O. Poncelet, C.
Aristegui, J. Leng, B. Mascaro, K. Zimny**

**CTRE NAT DE LA RECHERCHE SCIENTIFIQUE
1, ESPLANADE DES ARTS ET METIERS
TALENCE, 33400
FRANCE**

EOARD GRANT #FA8655-12-1-2067

Report Date: March 2014

Final Report from 1 March 2012 to 31 October 2014

Distribution Statement A: Approved for public release distribution is unlimited.

**Air Force Research Laboratory
Air Force Office of Scientific Research
European Office of Aerospace Research and Development
Unit 4515, APO AE 09421-4515**

REPORT DOCUMENTATION PAGE				Form Approved OMB No. 0704-0188	
<small>Public reporting burden for this collection of information is estimated to average 1 hour per response, including the time for reviewing instructions, searching existing data sources, gathering and maintaining the data needed, and completing and reviewing the collection of information. Send comments regarding this burden estimate or any other aspect of this collection of information, including suggestions for reducing the burden, to Department of Defense, Washington Headquarters Services, Directorate for Information Operations and Reports (0704-0188), 1215 Jefferson Davis Highway, Suite 1204, Arlington, VA 22202-4302. Respondents should be aware that notwithstanding any other provision of law, no person shall be subject to any penalty for failing to comply with a collection of information if it does not display a currently valid OMB control number.</small> PLEASE DO NOT RETURN YOUR FORM TO THE ABOVE ADDRESS.					
1. REPORT DATE (DD-MM-YYYY) 6 March 2014		2. REPORT TYPE Final Report		3. DATES COVERED (From – To) 1 March 2012 - 31 October 2014	
4. TITLE AND SUBTITLE Toward ultrasonic tunable ultra-damping metamaterials				5a. CONTRACT NUMBER	
				5b. GRANT NUMBER FA8655-12-1-2067	
				5c. PROGRAM ELEMENT NUMBER 61102F	
6. AUTHOR(S) Oliver Mondain-Monval, O. Sandre, T. Brunet, O. Poncelet, C. Aristegui, J. Leng, B. Mascaro, K. Zimny				5d. PROJECT NUMBER	
				5d. TASK NUMBER	
				5e. WORK UNIT NUMBER	
7. PERFORMING ORGANIZATION NAME(S) AND ADDRESS(ES) CTRE NAT DE LA RECHERCHE SCIENTIFIQUE 1, ESPLANADE DES ARTS ET METIERS TALENCE, 33400 FRANCE				8. PERFORMING ORGANIZATION REPORT NUMBER N/A	
9. SPONSORING/MONITORING AGENCY NAME(S) AND ADDRESS(ES) EOARD Unit 4515 APO AE 09421-4515				10. SPONSOR/MONITOR'S ACRONYM(S) AFRL/AFOSR/IOE (EOARD)	
				11. SPONSOR/MONITOR'S REPORT NUMBER(S) AFRL-AFOSR-UK-TR-2015-0011	
12. DISTRIBUTION/AVAILABILITY STATEMENT Distribution A: Approved for public release; distribution is unlimited.					
13. SUPPLEMENTARY NOTES					
14. ABSTRACT The intent of the research was to develop metamaterials with large attenuation capacities in a targeted field of frequencies, reducing the size of the resonators from the centimeter-level used in audible frequencies to microresonators able to function at ultrasonic frequencies, focusing on two approaches. The "core-shell" approach aimed to construct objects composed of a hard core showing a high density contrast with its surrounding elastic soft shell, the result embedded in a hard matrix. The second ("resonant-emulsion") approach aimed at fabricating a material in which the incoming wave exhibits a "Mie" resonance with the inclusions due to the sound velocity contrast between the inclusions and surrounding matrix. For efficiency we focused on the resonant-emulsion approach, fabricating a soft material composed of oil emulsion droplets suspended in a liquid water-based gel, allowing us to vary the average size and droplet volume fraction in the material. Applying a wave frequency to this material indeed showed variable attenuation at different wavelengths. Varying the droplet diameters allowed polydispersity in the material, reducing the individual scattering peaks and applying the attenuation coefficient to a broader range of frequencies. By doping the material with ferrofluid we hoped to specifically tune the local Mie resonance frequencies to set ultradamping at particular frequencies (for adaptive filters and acoustic mirrors or other applications), and research bifurcated into synthesis of fluorinated ferrofluid, and acoustic measurements of the obtained material. Once the ferrofluid was synthesized, application of the magnetic field elongated the droplets, shifting resonance peaks to higher frequencies, and this attenuation strongly changes from one geometry to another (whether droplets were elongated perpendicular or parallel to the arriving waves). Research now looks to synthesize and investigate materials for more intense scattering such as silicon polymers with template holes.					
15. SUBJECT TERMS EOARD, metamaterials, ultrasonic, Mie resonance					
16. SECURITY CLASSIFICATION OF:			17. LIMITATION OF ABSTRACT SAR	18, NUMBER OF PAGES 22	19a. NAME OF RESPONSIBLE PERSON Victor Putz
a. REPORT UNCLAS	b. ABSTRACT UNCLAS	c. THIS PAGE UNCLAS			19b. TELEPHONE NUMBER (Include area code) +44 (0)1895 616013

October 2014 report on the EOARD projects FA8655-11-M-4006 and FA8655-12-1-2067

**FA8655-11-M-4006: “Acoustic metamaterials through a microfluidic, bottom-up approach: Toward highly attenuating, negative effective density materials”
(October 2011 - October 2012)**

PI: A. Aradian (CRPP);

Associates: O. Mondain-Monval, S. Raffy (CRPP), T. Brunet (I2M), J. Leng (LOF),
B. Mascaro (USAF postdoc I2M/CRPP)

**FA8655-12-1-2067: “Toward ultrasonic tunable ultra-damping metamaterials”
(October 2012 - October 2014)**

PI: O. Mondain-Monval (CRPP);

Associates: O. Sandre (LCPO), T. Brunet, O. Poncelet, C. Aristégui (I2M), J. Leng (LOF),
B. Mascaro (USAF postdoc I2M/CRPP), K. Zimny (USAF postdoc LCPO/CRPP)

1) Our approaches

Our initial idea was to build metamaterials with specific properties such as large attenuation capacities in a targeted field of frequencies. If much work has been up to now performed using centimetre-sized handmade mechanical resonators adapted to audible frequencies [1-3], fewer attempts have been made on smaller micro-resonators, in the 100 μm range, i.e. for ultrasonic frequencies. Following this path, we recently proposed two different microfluidic approaches to get such micro-resonators:

1. The “core-shell” approach
2. The “resonant emulsion” approach

In the first one, we aimed at fabricating core-shell objects composed of a hard core exhibiting a high density contrast with a surrounding elastic soft shell, the resulting core-shell being finally embedded in a relatively hard solid matrix. Predictions [4] and earlier experimental results [1] show that, at a given frequency, the core-shell particle behaves as an oscillator which resonates with the incoming acoustic wave. The expected resonance occurs in that case at low frequency $f_{\text{res}} \sim 1/a$.

In the second approach, one aims at fabricating a material in which the incoming wave will exhibit a “Mie” type of resonance with the inclusions. In such case, the expected cavity resonance is due to the sound velocity contrast between the inclusions and the surrounding matrix. Resonance occurs at a frequency $f_{\text{res}} \sim ((n+1)/2) \cdot (c/a)$ where c and a are respectively the sound velocity in the inclusion and its characteristic size and n , an integer, the order of the resonance. Of course, significant resonating effects may only occur if the sound contrast between the inclusion and its surrounding medium is large enough, as noted by Li *et al* [5]. Earlier experimental works showed that interesting resonating behaviour can be obtained with air bubbles [6]. However, air bubbles are hardly stable in time and we proposed an alternative experimental route to achieve materials containing only liquids.

2) October 2011 – May 2012: the resonant emulsions approach

For the sake of efficiency and considering the time schedule of this USAF project, we decided to concentrate our efforts on the second approach which consists in fabricating a soft material composed of oil emulsion droplets (made with of fluorinated oil) suspended in a liquid water-based gel. We indeed identified that fluorinated oil (FC40) possesses a rather low sound speed for a pure liquid ($c = 640$ m/s) and performed some materials composed of micrometric oil droplets suspended in a Bingham fluid (a fluid that does behave as a solid under a given threshold stress, in our case a solution of polyacrylic acid (carbopol) in water) that has a sound speed of ~ 1500 m/s. An example of such a material obtained through a microfluidic approach is shown on figure 1. In this approach, one can vary the average size and droplets volume fraction in the material.

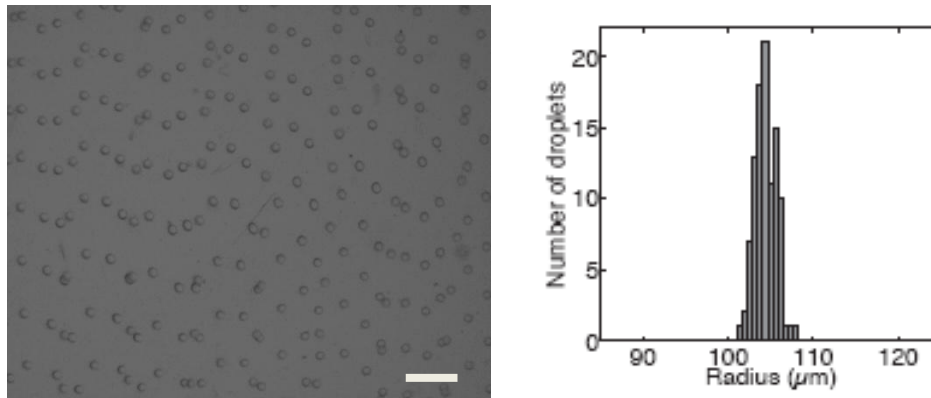


Figure 1:

a. Optical microscopy picture of FC40 oil droplets dispersed in a carbopol/water mixture (scale bar: 1mm); *b.* Corresponding droplets size distribution.

Within the frame of this USAF project, the hired postdoc (Benoit Mascaro) developed the experimental set-up required for the acoustic measurements inside the fluid (see figure 2).

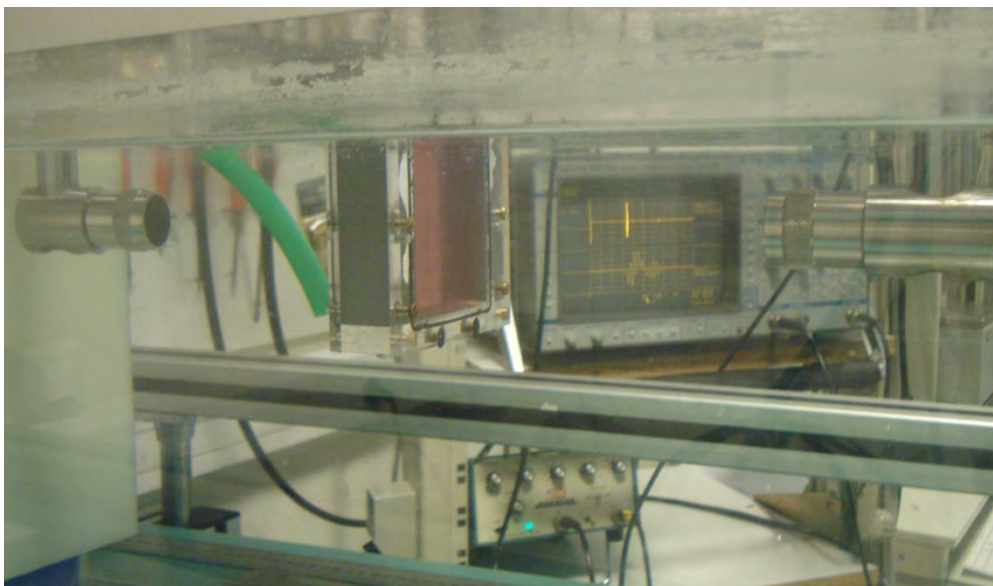


Figure 2:

Picture of the acoustic experimental set-up. The acoustic transducers are both immersed in water.

On this picture a 2.5 cm-thick plastic cell containing the material is introduced between an acoustic emitter and a receptor and both the acoustic attenuation and the phase velocity are measured as a function of the wave frequency f that is, in that case, varied between 1 and 10 MHz. On figure 3, we report the measurements performed in a material containing $\phi_V = 0.23$ vol % of droplets with average diameters $2R = 104 \pm 1 \mu\text{m}$. The measure clearly evidences the resonating behavior of the system. The different attenuation peaks corresponds to different orders n (the size of the inclusion being equal to an integer number of half wavelengths). The results could be fitted using the Independent Scattering Approximation (ISA) [7] that considers no interactions between the acoustic waves scattered by the inclusions. Leaving $2R$ and ϕ_V as the only free parameters of the fit, one gets an excellent agreement (solid lines on figure 3) with the data with $2R = 103.5 \mu\text{m}$ and $\phi_V = 0.22\%$, i.e some values very close to the ones obtained by the analysis of optical microscopy pictures [8]. The agreement is even better when the experimental droplets polydispersity is taken into account in the calculation (see dashed line in figure 3).

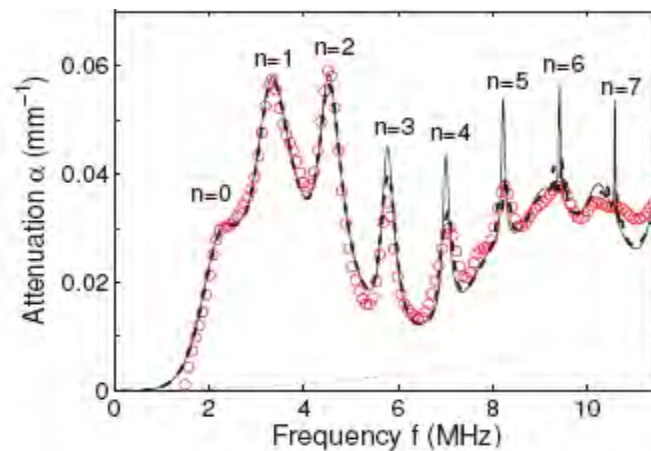


Figure 3:

Evolution of the attenuation coefficient (mm^{-1}) as a function of the wave frequency (MHz). Solid line: fitting of the data to the ISA model using $2R = 103.5 \mu\text{m}$ and $\phi_V = 0.22\%$ and considering no polydispersity; Dashed line: fitting of the data to the ISA model and taking into account the sample polydispersity.

3) May 2012 – October 2012: Impact of polydispersity on the resonant behavior

From May to October 2012, we have investigated the impact of polydispersity on multipolar resonant scattering. To achieve samples with controlled polydispersities, we performed droplets with slightly different diameters using the process described in section 2 and mix them together. This way, we could obtain targeted particle size distribution (PSD) as presented in figure 4. The PSD of each sample was characterized by optical measurements on about a hundred fluorinated-oil droplets. The mean radii $\langle a \rangle$ were about a hundred microns and the size-polydispersities $\sigma/\langle a \rangle$ ranged from 1% to 13% (see Fig. 4). The latter parameter can also be viewed as a quality factor $Q_{\text{PSD}} = \langle a \rangle / \sigma$. The volume fraction ϕ_V of oil-droplets was intentionally fixed to values as low as 1% in order to facilitate the experiments. The acoustical measurements of the attenuation coefficient and phase velocity for each sample are displayed versus the adimensional frequency as illustrated in Fig. 4. The mean radius of the oil droplets dispersed in each sample being not identical, the representation versus the reduced frequency ka is the most appropriate for a direct comparison between the resonant scattering of the different emulsions. By using an inversion technique based on a least squares optimization a best fit procedure permits the evaluation of the parameters characterizing the PSD: the mean radius $\langle a \rangle$,

the size polydispersity $\sigma/\langle a \rangle$ and the volume fraction ϕ_v , from the acoustic measurements. The values determined by optical and acoustical measurements summarized in Tab. I have been found to be very close. In particular, the size polydispersities of samples are well-recovered by acoustical measurements. Thus, the resonant regime could provide an accurate method to characterize the complete PSD of particulate mixtures such as emulsions or suspensions, usually studied in the long wavelength regime.

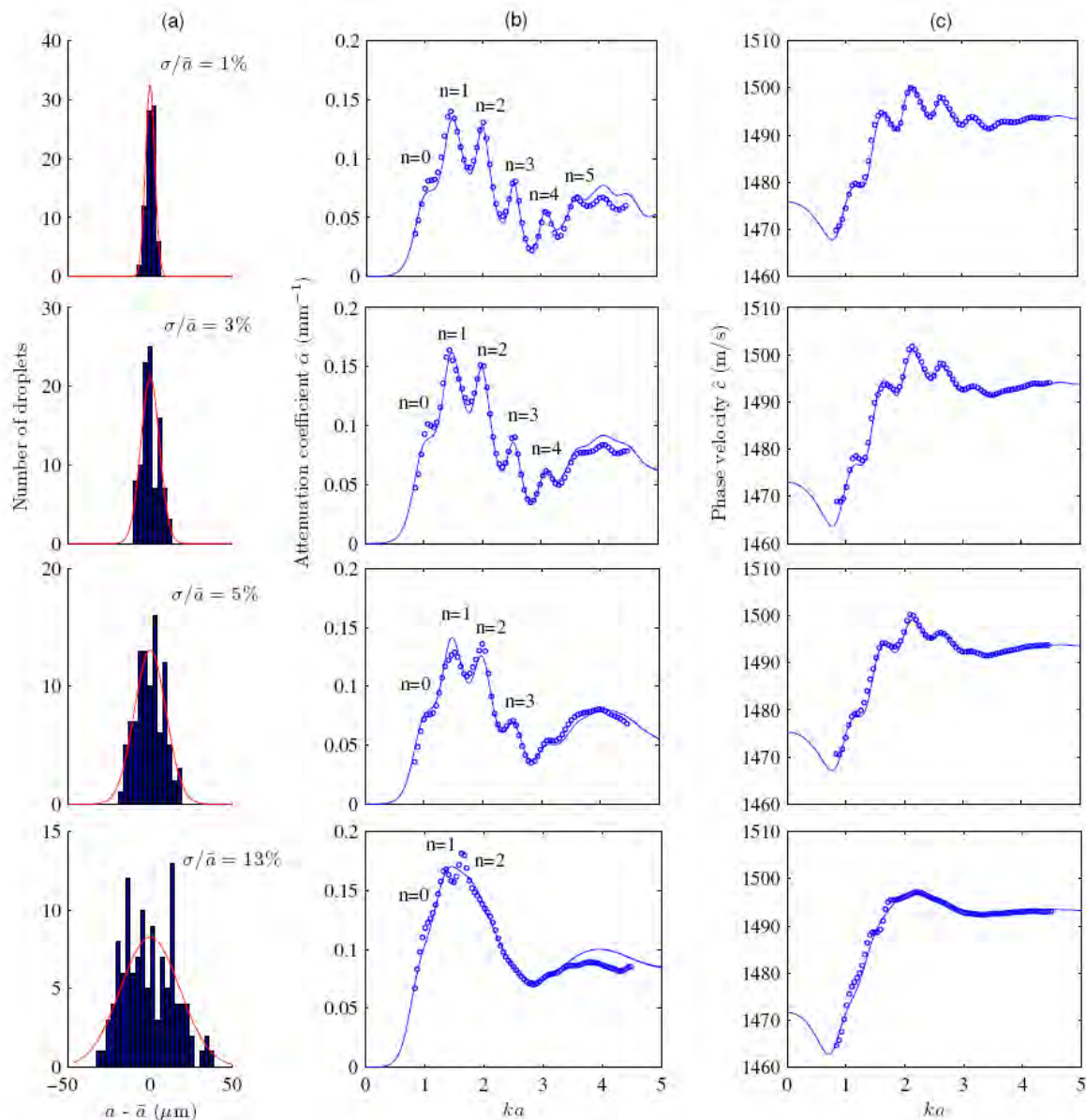


Figure 4:

Optical and acoustical properties of the emulsion samples with increasing polydispersity. (a) centered droplet-radius histograms obtained from optical microscopy measurements. (b) attenuation coefficient and (c) phase velocity: (o) acoustical measurement and (solid line) computations from the optimal polydisperse gaussian distribution (best fit of the experimental data to the model).

Sample number	$\langle a \rangle_{opt}$ (μm)	$(\sigma/\langle a \rangle)_{opt}$ (%)	$\phi_{V,opt}$ (%)	$\langle a \rangle_{ac}$ (μm)	$(\sigma/\langle a \rangle)_{ac}$ (%)	$\phi_{V,ac}$ (%)
1	185	1.4	≈ 1	181	2.41	0.95
2	174	3.1	≈ 1	173	3.6	1.1
3	172	4.9	≈ 1	170	4.82	0.98
4	128	12.7	≈ 1	142	13.4	1.19

Table I:

Compared values of the size, size distribution and volume fraction deduced from optical observations and acoustic characterization

Fig. 4 also shows that the scattering resonant features progressively disappear as the size polydispersity increases. For example, the attenuation peaks are clearly observable until $n = 5$ for the 1%-polydisperse emulsion (sample 1) while the fundamental resonances of the first three modes ($n = 0; 1; 2$) are hardly identifiable for a 13%-polydisperse emulsion (sample 4). Tab. II makes an inventory of the observable (o) or non observable (X) attenuation peaks for each sample. The narrowness of the resonance peaks is characterized by the quality factor $Q_{res} = f_{res}/\Delta f_{res}$, of which values are reminded in Tab. II. Thus, the two parameters Q_{res} and Q_{PSD} can be quantitatively compared for all resonances occurring in each sample. Tab. II shows then that Q_{PSD} must be higher than Q_{res} in order to clearly observe a distinguishable attenuation peak. All resonances, for which the quality factor Q_{res} is higher than Q_{PSD} , do not exhibit prominent features in the attenuation and phase velocity spectra.

	$n = 3$ $Q_{res} \approx 10$	$n = 4$ $Q_{res} \approx 24$	$n = 5$ $Q_{res} \approx 56$	$n = 6$ $Q_{res} \approx 140$
$\sigma/\langle a \rangle = 1\%$ $Q_{PSD} = 100$	O	O	o	X
$\sigma/\langle a \rangle = 3\%$ $Q_{PSD} = 33$	O	O	X	X
$\sigma/\langle a \rangle = 5\%$ $Q_{PSD} = 20$	O	X	X	X
$\sigma/\langle a \rangle = 13\%$ $Q_{PSD} = 7.5$	X	X	X	X

Table II:

Synthesis of observable (o) or non-observable (X) fundamental acoustic resonances of several modes ($3 \leq n \leq 6$) occurring in fluorinated oil droplet emulsions with different size polydispersities $\sigma/\langle a \rangle$ ranging from 1% to 13%. For comparison, the quality factor Q_{res} of these fundamental resonances are mentioned for each mode as well as the inverse of the size polydispersity, $Q_{PSD} = \langle a \rangle/\sigma$, which characterizes the particle-size distribution of the samples.

This simple approach thus provides a reasonable way to evaluate the impact of polydispersity on the resonance amplitude [9].

4) October 2012 – March 2013 : tunable resonant materials (Project FA8655-12-1-2067)

In the context of meta-materials, it is of prime importance to perfectly control the scattering resonances. Our results showed that the position of the resonance frequency scales as the inverse of the emulsion droplets size. Thus, to introduce a possible tuning of the acoustic response, we recently proposed to dope the emulsion droplets with a ferrofluid. Previous works indeed showed that magnetic emulsion droplets can change their shape and spatial organization when submitted to an external magnetic field [10, 11]. As a result, the local Mie resonance frequencies might be tuned in a very efficient and controlled way. Thus, we will be able to tune the effective acoustic properties of the emulsions, *e.g.* setting ultra damping at a particular frequency. Applications of such materials (as adaptative filters and acoustic mirrors) are numerous.

At this point, our project can thus be divided into two parts: 1) Synthesis of the fluorinated ferrofluid that would serve as “slow” deformable inclusions in the gel phase 2) Acoustic measurements in the obtained material with or without applied magnetic field.

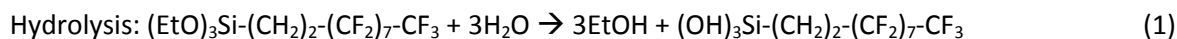
In October, we recruited a new postdoc on the chemistry part of our project (Kévin Zimny). Simultaneously, the contract also allowed for a 6-month prolongation of B. Mascaro’s contract on the part concerning the acoustic characterization of our samples. We now present the results obtained on each part:

4.1. Synthesis of the fluorinated ferrofluid and dispersion in the gel phase

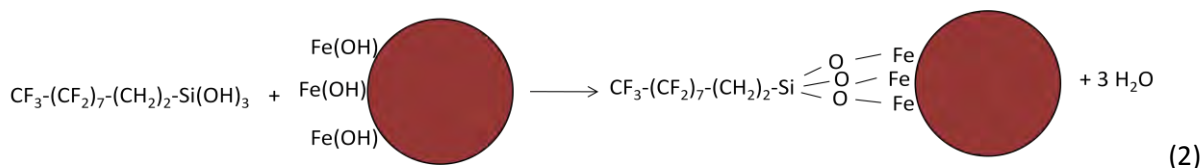
Maghemite nanoparticles ($\gamma\text{-Fe}_2\text{O}_3$) used in this work are prepared by coprecipitation of iron salts in alkaline media followed by an oxidation with nitric acid according to an aqueous iron^{II} and iron^{III} salts coprecipitation route also called ‘Massart’ procedure [12]. After synthesis, the nanoparticles are dispersed in water and their surface charge is positive in acidic conditions. The obtained magnetic nanoparticles (MNPs) have an average diameter of 30 nm (with a polydispersity index PDI = 0.04) and were used to prepare a fluorinated ferrofluid by a two-steps process. At first, the MNPs were coated with a perfluoropolyether end-functionalized with a carboxylic acid (Krytox 157-FSH, Dupont). Krytox was first mixed with a highly concentrated NH_3 aqueous solution and the ferrofluid was directly added to this mixture. In such conditions, the deprotonated carboxylic head of Krytox molecules have a negative charge and adsorb at the positively charged iron oxide surface. The obtained system was then washed several time with acetone in order to separate the Krytox covered MNPs from the polar mixture. Then, the obtained Krytox-MNPs mixture is dissolved in the fluorinated oil (perfluoro-2-butyltetrahydrofuran FC-75 from 3M). These fluorinated surfactant-based ferrofluids present a high viscosity (> 100 cP) incompatible with deposition through capillaries. This high viscosity is due to the relatively high viscosity of the FC75/Krytox continuous phase. In addition, the surface tension between the ferrofluid and a dilute carbopol solution (25 mN/m as measured using a pendant drop experiment) seems to be too high to observe a deformation of the droplets under a magnetic field of reasonable intensity (*i.e.* less than 600 Gauss).

Consequently, a second step of ligand exchange was performed in order to replace the Krytox 157-FSH surfactant by an organofluorosilane covalently grafted to the MNPs. The fluoroalkylsilane (1H,1H,2H,2H-perfluorodecyltriethoxysilane: $(\text{EtO})_3\text{Si}-(\text{CH}_2)_2-(\text{CF}_2)_7-\text{CF}_3$) that is miscible with FC75 was added directly to the surfactant-based ferrofluid in FC-75. Simultaneously a concentrated aqueous solution of Tetramethylammonium hydroxide ([TMAOH] = 0.1 M) was incorporated and strongly stirred in the ferrofluid mixture. The mixture was placed under stirring (300 rpm) for 3 days at 70°C,

In such conditions, we expect the following two steps sol-gel reaction to occur at the surface of the particle.

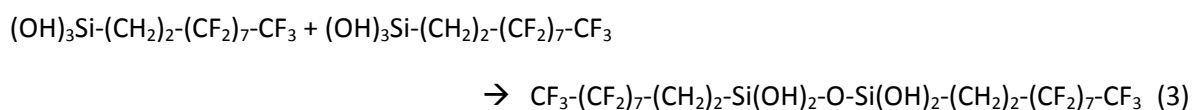


Condensation at the surface of the MNPs:



where TMAOH acts as a catalyst.

Of course, other events can occur such as the condensation of two silanes together:



Any combination of reaction (2) and (3) is also possible. The obtained sample was washed several times with water, ethanol and acetone then isolated on magnets in order to remove the un-reacted silane. MNPs were finally dried in a vacuum oven during 1h at 80°C and then dispersed in fluorinated oil FC-75. We call this ferrofluid a silanized ferrofluid.

The sample was then examined using IR spectroscopy. Figure 5 shows the IR spectra obtained for a) pure krytox b) silanized ferrofluid c) pure perfluodecyltriethoxysilane after sol-gel reaction. Several conclusions can be deduced from the comparison of these two spectra: i) In spectrum b), the presence of the band at 1070 cm^{-1} can be ascribed to the formation of Si-O-Si covalent bonds; ii) In spectrum b), the presence of the band characteristic of krytox molecules indicates that some of them remain on the MNPs surface. Unfortunately, there are as far as we know no easy way to evidence the presence of Fe-O-Si bonds. The presence of the Si-O-Si bonds around the MNPs tends to show that the silane are at least polymerized in the vicinity of the particles surface and that these inorganic polymer chains are somehow enough linked to the surface so that the washing procedure does not separate the particles from the silane molecules.

The effect of the two coatings on the colloidal stability of the MNP dispersion in FC-75 was studied using small angle neutron scattering (SANS). SANS experiments were performed on much smaller MNPs ($\sim 5\text{-}7 \text{ nm}$ diameter from TEM). Figure 6 shows that the ferrofluid coated by Krytox (after the first step) is prone to aggregation as can be seen from the constant increase of the intensity at low q vectors. On the contrary, the silanized MNPs spectrum exhibits a Guinier plateau at low q values. Such a difference between the two spectra allows one to conclude that the dispersion is more stable in the second case since the particles endure a stronger interparticle repulsive force due to the presence of the silane corona. Furthermore, this spectrum can be fitted to the form factor expression for a core-shell particle in which the free parameters of the fit are the radius of the inorganic iron core R_0 and the hydrogenated shell thickness t_0 . The best fit of our data to the model leads to $R_0 = 2.6 \text{ nm}$, in good agreement with TEM, and $t_0 = 1.42 \text{ nm}$. We used the reported values for the neutron scattering length densities: $\rho_{\text{core}} = 6.98 \times 10^{10} \text{ cm}^{-2}$ for the iron oxide core, $\rho_{\text{shell}} = 1.53 \times 10^{10} \text{ cm}^{-2}$ for the hydrogenated shell and $\rho_{\text{FC-75}} = 3.84 \times 10^{10} \text{ cm}^{-2}$ for the FC-75 continuous phase.

Thus, these SANS experiments (performed at LLB-CEA Saclay France) indicate that the grafting of a fluorosilane onto the MNPs greatly improved the quality of the dispersion in the fluorinated oil. Surface tension measurements (performed using the pendant drop experiment) also showed a decrease of the interfacial tension between the silanized ferrofluid and a dilute Carbopol solution by a factor about 2 (11 mN/m). Thus, a high deformation of the silanized ferrofluid in Carbopol gel could be observed under magnetic fields varying from 0 to 600 Gauss (Figure 7). Such a varying field could be obtained using a small electromagnetic coil coupled to the optical microscope. The observed deformation of the ferrofluid droplet is characterized by the evolution of the droplet axial ratio $a_{//}/a_{\perp}$ as a function of the applied magnetic field. In this case, $a_{//}/a_{\perp}$ reached a value of 2.4 under a magnetic field of 600 gauss. This observation is in sharp contrast with the previous tests performed with the krytox coated-ferrofluid for which no deformation was observed under this type of magnetic field value. This is most probably due to the difference in surface tension measured from one system to the other. Let us also note that the droplet deformation is fully reversible and the droplet goes back to its spherical shape as the field is turned off [13].

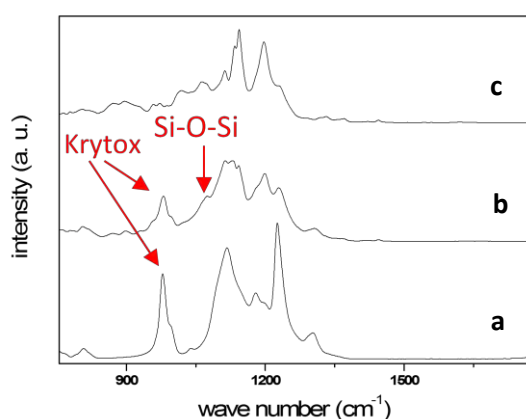


Figure 5:

IR –spectra of a) Pure Krytox;
b) Silanized Ferrofluid;
c) perfluodecyltriethoxysilane after sol-gel

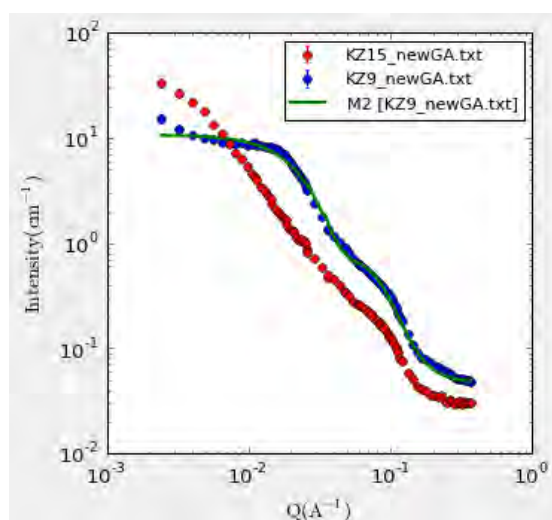


Figure 6:

SANS curves of the surfacted ferrofluid (KZ15) and the silanized MNPs (KZ9).

For the purpose of acoustic measurements, ferrofluid emulsions in carbopol solutions (figure 8a) were prepared by injecting a 6 vol % concentrated ferrofluid oil through a silica capillary ($d=40 \mu\text{m}$) in the gel (Carbopol 0.05 % w/w) with a controlled pressure of 1.7 bar and using the previously described robotic approach [6, 8, 9]. The yield stress of the used Carbopol gel (which depends on its concentration in water) was measured at 1.5 Pa for a concentration of 0.05 % w/w using standard rheology. In such conditions, we calculated that ferrofluid droplets (mass density $\rho = 1.9 \text{ g/cm}^3$) can stay suspended as long as their diameter is lower than $250 \mu\text{m}$. The sizes of the emulsion droplets were measured optically and presented a mean radius of $105 \mu\text{m}$ and dispersity $\sigma/\langle a \rangle = 4 \%$ (Figure 8b). The oil volume fraction of the final emulsion is typically around 1 %.

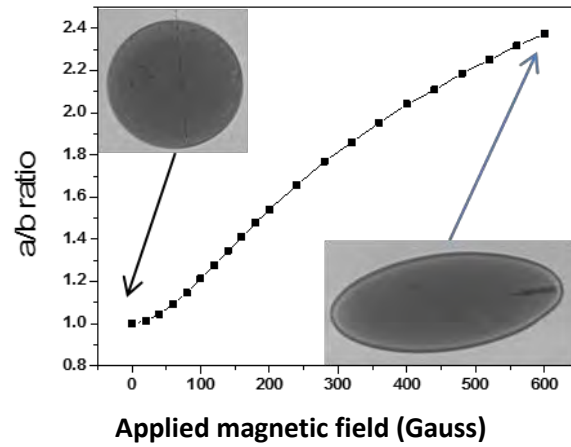


Figure 7:

Evolution of the axial aspect ratio $a_{//}/a_{\perp}$ of a silanized ferrofluid droplet as a function of the applied magnetic field. The prepared ferrofluid contained 6 vol % of iron oxide of average hydrodynamic diameter 47 nm (obtained from light scattering).

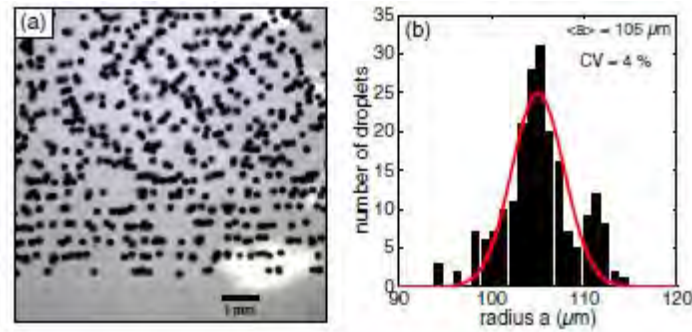


Figure 8:

(a) Optical microscopy picture of fluorinated ferrofluid droplets embedded in a water-based gel matrix, achieved by means of robotics ($\phi_v \sim 1\%$). (b) Corresponding histogram of the droplet-size distribution. Mean radius $\langle a \rangle = 105 \mu\text{m}$ and coefficient of variation $CV = 4\%$.

As done before, we used a multi-echo ultrasound spectroscopy technique to characterize the tunable emulsion. However, the transducer is here directly stuck on the measurement cell in order to place that system within the air gap of the magnet that is around 5 cm wide. First, the emulsion, made of fluorinated oil droplets doped with magnetic nanoparticles, has been acoustically characterized without applying an external magnetic field, providing reference results at rest (solid line in Fig. 9). Attenuation peaks are clearly evidenced as already observed in monodisperse emulsions made of pure fluorinated oil droplets (Fig. 3). Thus, the presence of magnetic nanoparticles within the oil droplets does not affect their resonant response.

To observe the acoustic behavior of the material in the presence of a magnetic field, we first used a combination of four permanent magnets, which position in space allows for the presence of a relatively homogeneous 600 G field in a $5 \times 5 \times 5 \text{ cm}^3$ volume. Unfortunately, this method does not permit to progressively vary the value of the external field but is a first way to evaluate the influence of the droplet shape on the acoustic spectrum. By turning the measurement cell containing the sample in the air gap of the magnet, the applied magnetic field can be either parallel or perpendicular to the incoming acoustic wave. In both cases, the initially spherical droplets clearly deform and become ellipsoidal with an aspect ratio of about 2 for an applied magnetic field of 600 Gauss (see Fig. 7 and the pictures of Fig 9).

The recorded spectra are displayed as dashed lines on fig 9. Our first observation is that the attenuation spectrum is drastically impacted by the deformation of the resonant magnetic droplets. At given frequencies, the attenuation value is changed by a factor of 2 and even a factor of 4 as the field direction is changed from being perpendicular to parallel to the wave direction of propagation. These results are very recent and we still work on understanding the evolution of the spectrum as the field is applied.

We can however note that:

- i) The resonance peaks shift to higher frequencies when the droplets are elongated perpendicular to the direction of propagation of the incoming wave. At first order, such an effect can be attributed to a decrease in droplet dimension in the direction of propagation of the acoustic wave. Indeed, as we showed before [8], the resonance frequencies are inversely proportional to the droplets size (Fig 10). This must also be the reason why the frequency position seems to decrease in the other case, i.e. when droplets elongate in the wave direction of propagation (Fig 10).
- ii) The attenuation observed at high frequencies strongly changes from one geometry to the other. One possible explanation would be that the scattering cross-section is higher in the perpendicular case than in the parallel one (see Fig 10).

These first experiments validate our approach and show that the acoustic properties of our material can be tuned by the application of an external field.

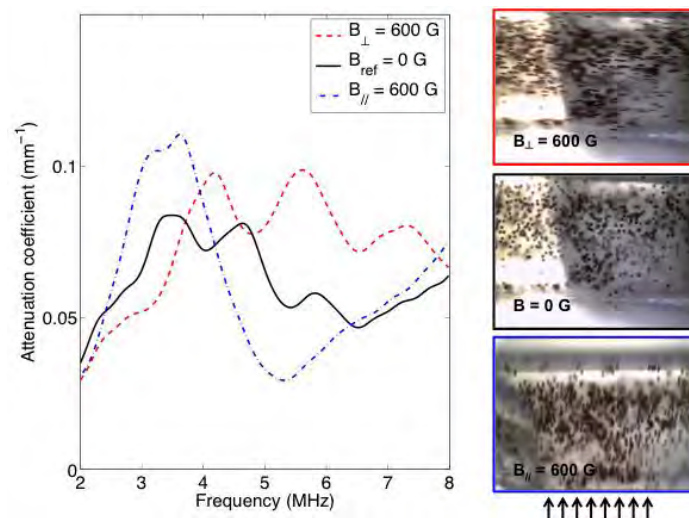


Figure 9:

Attenuation coefficients (mm^{-1}) for emulsions of magnetic fluorinated droplets submitted to an external magnetic field ($B = 600 \text{ G}$), parallel or perpendicular to the incoming acoustic wave (arrows). Corresponding optical microscopy pictures illustrating the droplet deformations under the magnetic field.

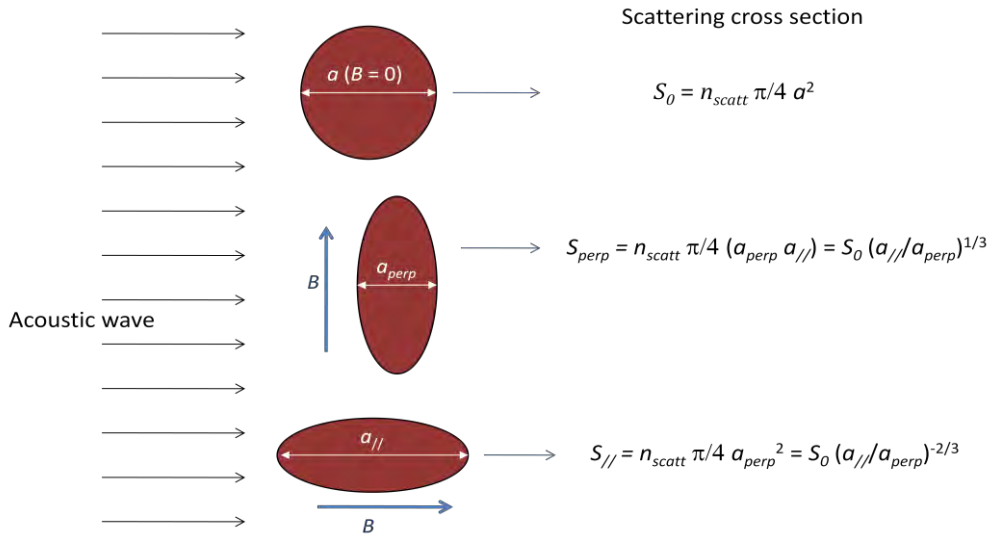


Figure 10:

Schematic representation of the ferrofluid droplets submitted to the magnetic field in the two different geometries. n_{scatt} is the number of droplets in the sample. One obtains $a_{perp} < a (B=0) < a_{//}$ and $S_{//} < S_0 < S_{perp}$

5) March 2013 – March 2014: Experiments and model on tunable systems

As a follow-up of this work, we performed the full chemical characterization of the ferrofluid, and the measurement of the acoustic properties as a function of the magnetic field intensity and orientation with respect to the incoming acoustic wave.

5.1. Full physico-chemical characterization of the synthesized ferrofluid and droplets

We were in particular interested in measuring the magnetic susceptibility of the ferrofluid. This step is compulsory in order to predict the evolution of the droplet aspect ratio as a function of the applied field and the interface surface tension. The following results were published recently [13].

Magnetometry. The magnetization curves of silanized MNPs were obtained from superconducting quantum interference device (SQUID) magnetometry measurements at 300K (Fig. 11). After subtracting the diamagnetic contribution of the solvent, the magnetization curve $M(H)$ follows a Langevin law describing the progressive orientation of the magnetic moments along the magnetic field followed by their saturation at a plateau value M_s . This saturation magnetization reads $M_s = \phi \cdot m_{spe}$, where m_{spe} is the specific magnetization approximately equal to $3 \times 10^{-5} \text{ A} \cdot \text{m}^{-1}$ for colloidal maghemite nanoparticles and ϕ is the MNPs volume fraction (the magnetization being defined as the volume density of magnetic moments). This superparamagnetic behavior in the liquid state directly evidences that the silanization reaction at the surface of the MNPs enabled their stabilization against aggregation up to a magnetic field induction as high as 7 T. The magnetic susceptibility defined as the slope of the magnetization curve at low field was $\chi = 0.05$ for this sample diluted at $\phi = 1\%$. Therefore, the susceptibility of sample at any volume fraction can be calculated by $\chi = 5 \cdot \phi$. The exact shape of the measured magnetization curve $M(H)$ could be fitted by the convolution of the Langevin law of superparamagnetism with a size distribution of the MNPs for which we assume a log-normal law.

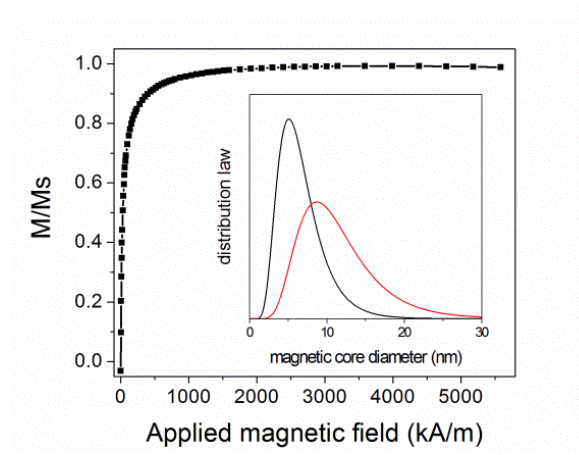


Figure 11:

Magnetization curve of the PFDTs-silanized ferrofluid sample in FC-75 ($\phi = 1\%$ v/v) by SQUID normalized by the saturation value at high field; inset: Log-normal distribution of magnetic inorganic core diameters: by number (black line) and by volume (red line)

Using this method, we obtained a median diameter $d_0^{\text{SQUID}} = 6.1$ nm and a logarithmic size width $\sigma^{\text{SQUID}} = 0.42$. The inset of Fig. 10 a) shows the particle size distribution by number ($d_n^{\text{SQUID}} = 6.7$ nm) and by volume ($d_w^{\text{SQUID}} = 11.4$ nm). These two values are both smaller than those obtained by TEM images analysis ($d_n^{\text{TEM}} = 10.2$ nm and $d_w^{\text{TEM}} = 19.1$ nm). This difference is ascribed to the reported presence of a nonmagnetic dead layer around ferrite MNPs and to the silicon-rich shell that is visible on TEM images but does not contribute to the magnetic properties.

5.2. Extensive study of the acoustic response in magnetic fields of various intensity and orientation

First, we did set up a new acoustic cell able to produce a homogeneous and tunable magnetic field on a $5 \times 5 \times 5 \text{ cm}^3$ domain. We adapted a coil to the acoustic set up and we were able to study the evolution of the acoustic response as a function of the applied field intensity and orientation with respect to the acoustic wave. The sample is confined in a 5 mm thickness acoustic measurement cell with small lateral dimensions ($30 \times 30 \text{ mm}^2$), on which a piezoelectric transducer of 5 MHz central frequency and 0.50 in. diameter has been stuck as illustrated in Fig. 12. Since its surface is sufficiently large, the piezoelectric transducer measures the wave field averaged over its face. Moreover, the incoherent part of the acoustic field is negligible as we only consider dilute emulsions with volume fractions ϕ_v of about 1%, in order to avoid coalescence between droplets when they elongate under the external magnetic field. Thus, the remaining detected signal is the coherent wave. The cell-transducer ensemble just takes up the width of the air gap (40 mm) of an electromagnet that generates a homogeneous magnetic field of which induction can be precisely tuned up to $B = 43$ mT. The measurement cell can also be turned along with its vertical axis to vary the angle ζ between the direction of the magnetic field B and the acoustic wave vector k_0 (Fig. 12(a)). Acoustic experiments are then performed using multi-echo ultrasound spectroscopy techniques allowing accurate measurement of the effective acoustic attenuation coefficient for the emulsion.

A first acoustic experiment is performed on the fluorinated ferrofluid droplet emulsion without applying any magnetic field (thickest blue lines in Fig. 13).

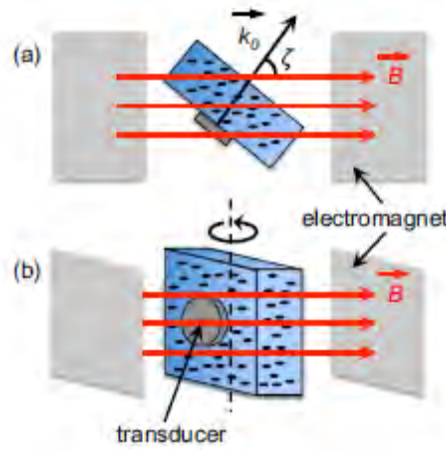


Figure 12:

(a) Top and (b) side views of the experimental setup dedicated to acoustic measurements on fluorinated ferrofluid droplet emulsions under magnetic fields with various inductions (up to 43 mT) and orientations. The angle ζ between the direction of the magnetic field B and the acoustic wave vector k_0 can be varied between 0° and 90° .

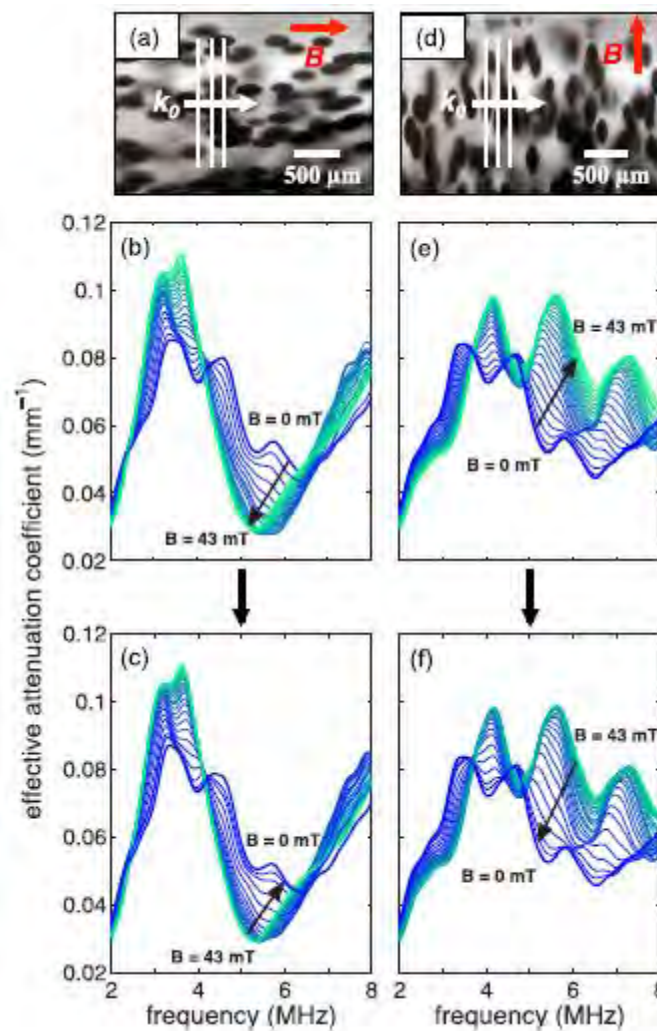


Figure 13:

Evolution of the attenuation frequency spectra of fluorinated ferrofluid droplet emulsions submitted to a cycle of increasing (b),(e) and decreasing (c),(f) magnetic field inductions (from 0 to 43 mT). The direction of the magnetic field B is parallel (a)–(c) or perpendicular (d)–(f) to the incident acoustic wave vector k_0 . Thickest curves refer to the reference emulsion made of spherical droplets (no magnetic field). Panels (a) and (d) show the orientation of the fluorinated ferrofluid droplets along the direction of the magnetic field B

The attenuation spectra clearly exhibit several peaks that are due to the multipolar Mie resonances of the spherical droplets. From such an acoustic resonant response, an inverse procedure provides an acoustically measured mean radius $\langle a \rangle$ of 106 μm and a coefficient of variation of 5%, in excellent agreement with optical microscopy measurements (Fig. 8). Then, the attenuation spectra are recorded for a cycle of increasing and decreasing magnetic field inductions with a 20 s delay between two acoustic measurements. When the direction of the applied magnetic field B is parallel to the acoustic wave vector k_0 (Fig. 13a), the attenuation spectrum tends to shrink down towards lower frequencies (Fig. 13b). By contrast, the attenuation peaks clearly shift towards higher frequencies (Fig. 13e) when the magnetic field B is applied perpendicularly to the acoustic wave vector k_0 (Fig. 13d). In both configurations, the initial attenuation spectra are fully recovered after cancellation of the magnetic fields (Figs. 13c and 13f). As suggested by the hysteretic loop shown in Fig. 7, the initially spherical droplets become spherical again after being elongated into prolate spheroids with an axial aspect ratio of 2.5 for the highest magnetic field induction. Therefore, the effective acoustic parameters of the emulsion can be reversibly tuned over a broad range of values.

Then, we model the scattering by the deformed objects using a much less naïve description than the one exposed in Fig. 10. Since the volume fraction of droplets for the considered emulsion is quite low ($\phi_v \sim 1\%$), the experimental results are analyzed within the framework of the independent scattering approximation. Indeed, cross correlations between scatterers do not need to be taken into account contrary to more concentrated media or random media made of strongly resonant particles such as air bubbles. Thus, the effective attenuation coefficient α_{eff} of the coherent pressure wave propagating in our dilute emulsion is given by [15]:

$$\alpha_{\text{eff}} = \frac{2\pi}{k_0} \int_a \varphi(a) \text{Im}[F_a(0)] da$$

where k_0 is the incident wave number in the host matrix, $\varphi(a)$ is the number of a -radius droplets per unit volume and $F_a(0)$ is the forward scattering function of a single droplet that depends on both the material properties of the particles and those of the host matrix. For a given couple of materials, the frequency locations of the resonant attenuation peaks are inversely proportional to the droplet size. As the coefficient α_{eff} depends on the forward scattering function $F_a(0)$, one can get an intuitive understanding of the evolution of the attenuation frequency spectra as a function of the magnetic field induction (Fig. 13) by considering only the droplet size along with the incident acoustic wave vector k_0 . When the magnetic field is parallel to the incoming acoustic waves, the droplets elongate along that direction (Fig. 13a) and the resonant attenuation peaks shift towards lower frequencies (Figs. 13b and 13c). Inversely, when the magnetic field is applied perpendicularly to the incoming acoustic waves, the droplet size become smaller along that direction (Fig. 13d) and the attenuation peaks shift towards higher frequencies (Figs. 13e and 13f). To go beyond such a qualitative analysis, the forward scattering function $F_a(0)$ of the prolate droplets has to be derived in order to retrieve the effective attenuation coefficient measured in our emulsions. Wave scattering by spheroidal objects has been the subject of many theoretical works [16], and the exact solution of the acoustic wave scattering by a liquid prolate spheroid was obtained many decades ago [17]. From the latter theoretical work, the forward scattering function $F_a(0)$ of a prolate fluorinated ferrofluid droplet whose axial aspect ratio a/b is 2 is calculated providing the effective attenuation coefficient of our emulsions submitted to an external magnetic induction B_0 of 25 mT (see Fig. 7) for various orientations ζ . Theoretical predictions and experimental measurements are compared for five angles ζ between the direction of the magnetic field B and the acoustic wave vector k_0 : $\zeta = 0^\circ$ (B_0 is parallel

to k_0), 22.5° , 45° , 67.5° , and 90° (B_0 is perpendicular to k_0) revealing an excellent quantitative agreement as shown in Fig. 14.

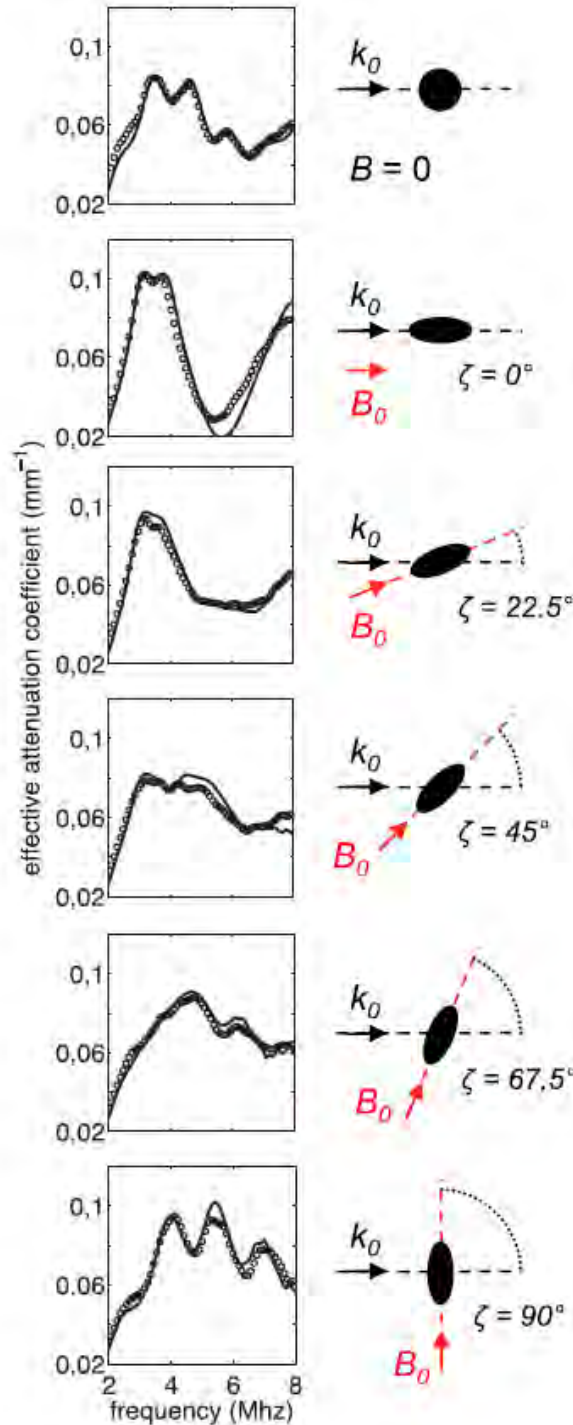


Figure 14:

Comparison between the measured attenuation coefficients (circles) and those predicted in the framework of the independent scattering approximation (solid lines) for emulsions made of prolate fluorinated ferrofluid droplets with an axial aspect ratio of 2. Various orientations between the direction of the magnetic field (of $B_0 = 25$ mT induction) and the acoustic wave vector k_0 are investigated ($\zeta = 0^\circ$, 22.5° , 45° , 67.5° , and 90°). The top figure refers to the reference emulsion made of spherical droplets (no magnetic field).

In conclusion, the resonant attenuation in our emulsion can be widely tuned (by a factor 5) by controlling both the flux density and the orientation of external magnetic fields. Such a tunability of the resonant properties of scattering media should be of the utmost relevance for metamaterials, of

which unusual properties are driven by scattering resonances [3]. As reported for electromagnetic waves, the use of magnetic fields turned out to be efficient to tune the effective permeability of metamaterials made of split ring resonators. This external stimulus should also be appropriate to tune the properties of locally resonant materials in acoustics [18], providing large enough mechanical contrasts between the resonant particles and the host matrix as expected with soft acoustic metamaterials [19]. These results were recently published in Physical Review Letters [20].

6) March 2014 – September 2014: looking for a new “slow” medium

As discussed above, the fluorinated emulsions do not allow for the achievement of very intense resonance scattering and, as a consequence, of strong “meta” effects. Thus, we started to search for new materials exhibiting lower phase velocity values.

The longitudinal sound speed of propagation c_L in a material reads: $c_L = 1/(\chi \cdot \rho)^{1/2}$ where χ is the isentropic compressibility and ρ the mass density. Low values of c_L thus imply both a large value of these two quantities. Possible candidates are polymer foams made out of material with a non zero density and the smallest possible compression modulus. Soft polymers as silicon polymers can be made porous by using the polyHipes (for Polymerizable High Internal Phase Emulsions) approach that consists in templating holes in the material using inverted water-in-oil emulsions. During this time period (March 2014 – October 2014), we showed that such silicon polymers can indeed be made porous using this approach.

Fabrication of the silicon monoliths: The polyHIPE approach was first developed during the 80s in the Unilever laboratories [21] and was later applied to produce the so-called polyHIPEs materials. Such materials are obtained by polymerization of a High Internal Phase Emulsion (HIPE), that is, dispersion of a large volume of internal phase in a continuous phase. A HIPE is characterized by an internal phase volume fraction ϕ greater than 74% of the total volume. This limiting value theoretically corresponds to the compact stacking of monodisperse rigid spheres. Above this ratio, the formation of a HIPE involves the deformation of the droplets into polyhedra surrounded by a thin film of continuous phase. In many cases of course, emulsions are not monodisperse but this volume fraction value still remains useful as the indication of the onset of the liquid spheres deformation. Then, the polymerization of the continuous phase somehow “freezes” the structure and the removal of the dispersed phase creates voids, or cells, in the material. In most cases, holes appear in the polymer film during the polymerization process and create connections between adjacent droplets of dispersed phase. As a consequence, the finally obtained polymer porous material has an opened cell structure, which allows for an easy drying of the system.

The continuous phase of the emulsions was performed by mixing a silicon based UV polymerizable fluids containing epoxy function (poly205 from BlueStar Silicone) together with a catalyzer (4 wt%), a UV sensitive molecules (ITX, 2 ppm) and a Poly(ethylene oxide) (PEO)-block-poly(dimethylsiloxane) (PDMS) surfactant (0.4 wt%). Then, a large proportion of brine ($[\text{NaCl}] = 1.3 \text{ wt\%}$) was progressively introduced in the system under shear. The final volume fraction of aqueous phase can be varied from 0 to 60 %. For such volume fractions below 70%, the materials are rather referred to as polyLIPE or polyMIPE for polymerized low (typical $\phi < 30\%$) or medium (typical $30\% < \phi < 70\%$) internal phase emulsions respectively. The prepared water-in-oil emulsions could be characterized using optical microscopy and light scattering. Typical diameters of the prepared emulsion droplets were found to be around 10 μm but smaller sizes could be reached by further injecting ultrasound in the system. Thus the emulsion diameters could be decreased to less than 1 μm . Unlike pioneering works on

PDMS porous materials [22, 23], polymerization of the continuous phase of these emulsions was achieved by shining UV to fluid cylindrical samples of diameter 30 mm and thicknesses between 1 and 5 mm. To avoid water evaporation during the polymerization process and achieve samples with smooth surfaces, the emulsions were introduced in PTFE molds of various thicknesses and maintained between two quartz plates. UV was applied during typically 2 minutes to each face of the sample. Thus, samples of very well defined thickness and smooth surfaces could be obtained (Fig. 15a). The samples were afterward stored at 60°C for 1 day to evaporate water. SEM picture of the internal part of the material reveals its porous structure (Fig. 15b).

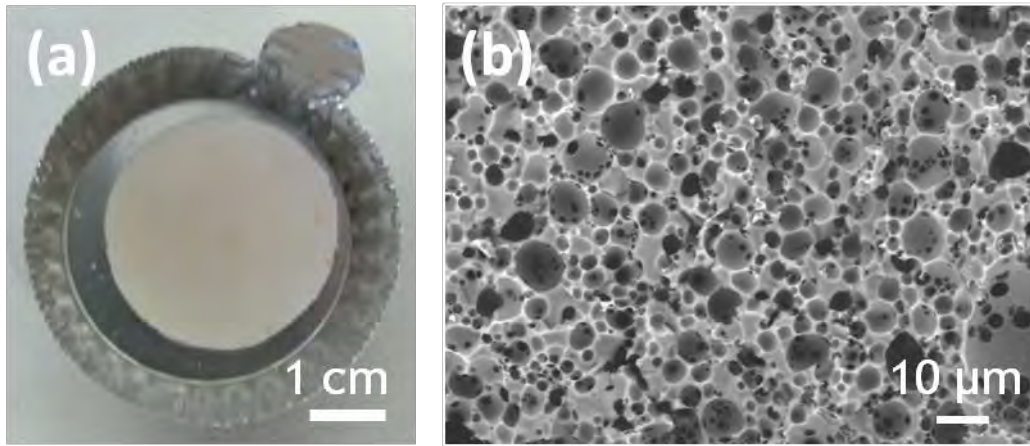


Figure 15:

Macroscopic (a) and SEM (b) picture of a porous silicon material obtained using the polyHIPEs approach

Acoustic characterization of the samples: The sound velocity was measured in samples of various porosities varying from $\phi = 0$ to around 40 %. The results are shown on figure 16. Two remarkable facts can be noticed: i) the velocity values very steeply decrease as the porosity of the material varies from 0 to low values as 10 % ii) The asymptotic value that is attained at large ϕ values is much lower (typically 100 m/s) than the one measured in air (340 m/s).

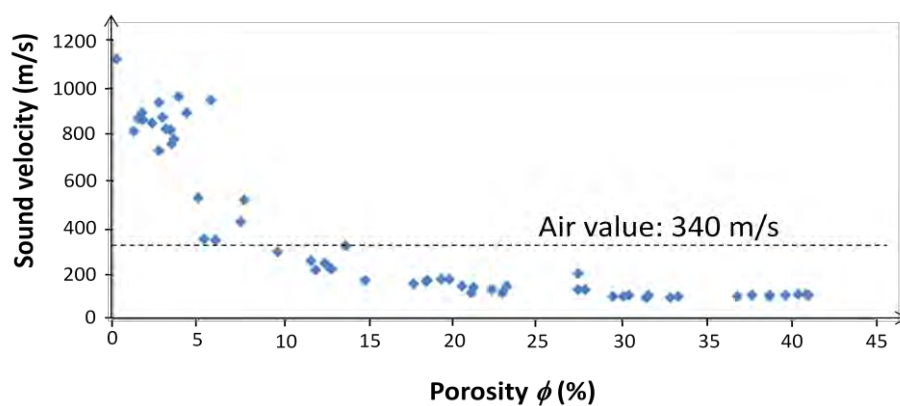


Figure 16:

Evolution of the sound velocity as a function of porosity ϕ in porous silicon samples

These measurements clearly show that, above a gas volume fraction of around 30%, the sound speed falls down to around 80 m/s thus making this material a very good candidate for the targeted application. In a project funded by the French research agency ANR, we did work on the shaping of

this material as porous beads to be used as resonators in the used fluid matrix. The results on that part have been recently submitted for publication [24]. We are also currently working on a model to describe the evolution of the sound speed in these types of porous media.

7) References

- [1] Z. Liu *et al*, *Science* **289**, 1734 (2000)
- [2] N. Fang *et al.*, *Nature Materials* **5**, 452 (2006)
- [3] Z. Yang *et al.*, *Applied Physics Letters* **96**, 041906 (2010)
- [4] Z. Liu *et al.*, *Physical Review B* **71**, 014103 (2005)
- [5] J. Li *et al.*, in *Physics of Negative Refraction and Negative Index Materials*, pp.183-215, edited by C.M. Krowne and Y. Zong (Springer, Berlin, 2007)
- [6] V. Leroy *et al.*, *European Physical Journal E* **29**, 123 (2009)
- [7] P. Sheng, *Introduction to Wave Scattering, Localization, and Mesoscopic Phenomena* (Springer, Heidelberg, 2006)
- [8] T. Brunet *et al.*, *Applied Physics Letters* **101**, 011913 (2012)
- [9] B. Mascaro *et al.*, *Journal of the Acoustical Society of America* **133** (4), 1996 (2013)
- [10] J.-C. Bacri *et al.*, *Journal de Physique Lettres* **43**, L649 (1982)
- [11] O. Mondain-Monval *et al.* *Physical Review Letters* **75** 3364 (1995)
- [12] R. Massart, *Comptes rendus de l'Académie des Sciences Série C* **291** (1), 1-3 (1980) ; J.P. Jolivet *et al.* *New Journal of Chemistry* **7** (5), 325 (1983)
- [13] K. Zimny *et al.*, *Journal of Materials Chemistry B* **2**, 1285 (2014)
- [14] A.O. Tsebers, *Magnetohydrodynamics* **21** (1), 19-26 (1985).
- [15] A. Ishimaru, *Wave Propagation and Scattering in Random Media* (Academic, New York, 1978)
- [16] C. Flammer, *Spheroidal Wave Functions* (Dover, New York, 2005)
- [17] C. Yeh, *J. Acoust. Soc. Am.* **42**, 518 (1967)
- [18] Z. Liu, X. Zhang, Y. Mao, Y. Y. Zhu, Z. Yang, C. T. Chan, and P. Sheng, *Science* **289**, 1734 (2000)
- [19] T. Brunet, J. Leng, and O. Mondain-Monval, *Science* **342**, 323 (2013)
- [20] T. Brunet *et al.*, *Physical Review Letters* **111**, 264301 (2013)
- [21] Barby, D.; Haq. Z., European Patent 0 060 138 (Unilever, applicant), (1982)
- [22] T. Kobayashi *et al.*, *J. Appl. Polym. Sci.* **50**, 971, 23 (1993)
- [23] MT Grosse *et al.*, *J. Pol. Sci. Part A Pol. Chem.* **46**, 21 (2008)
- [24] T. Brunet *et al.*, submitted

8) Participation to conferences

B. Mascaro: Oral presentation at Anglo-French Physical Acoustics Conference, 18-20 January 2012, Brighton, UK

T. Brunet: Poster at the international symposium on Ultrasound in the Control of Industrial Processes, 18-20 April 2012, Madrid, Spain

T. Brunet: Oral presentation at Acoustics 2012, 23-27 April 2012, Nantes, France

O. Mondain-Monval: Invited talk at the "International Conference on Materials Science and Technology", 10-14 June 2012, Kottayam, India

O. Mondain-Monval: Invited seminar for the *Dr R A Mashelkar Endowment Lecture Series in Advanced Materials*, June 8th 2012, National Chemical Laboratory, Pune, India

O. Mondain-Monval: Invited seminar, June 15th 2012, Indira Ghandi Center for Atomic Research, Kalpakkam, India

O. Mondain-Monval: Invited talk, International Bordeaux-UCLA Workshop, 28th Feb - 1st March 2013, Los Angeles, USA

O. Mondain-Monval: 2013 Annual Grantees'/Contractors' Meeting for AFOSR "Mechanics of Multifunctional Materials & Microsystems (M^{^4})", Arlington, USA, 16-19 December 2013

O. Mondain-Monval: invited seminar, Naval research Laboratory, 17 December 2013, Washington DC, USA (G. Orris)

O. Mondain-Monval: invited seminar, Laboratory for Research on the Structure of Matter, 20 December 2013, Philadelphia, Univ. of Pennsylvania, USA (A. Yodh)

T. Brunet: Oral presentation at International Congress on Ultrasonics, 2-5 May 2013, Singapore.

B. Mascaro: Oral presentation at Anglo-French Physical Acoustics Conference, 15-17 January 2014, Surrey, UK.

T. Brunet: Invited talk at Condensed Matter, 24-29 August 2014, Paris, France.

C. Aristégui: Invited talk at Metamaterials'2014, 25-30 August 2014, Copenhagen, Denmark.

K. Zimny: IOP conference on "The Physics of Soft and Biological Matter", 14-16 April 2014, Cambridge, UK

9) Publications

"Sharp acoustic multipolar-resonances in highly monodisperse emulsions", Thomas Brunet, Simon Raffy, Benoit Mascaro, Jacques Leng, Régis Wunenburger, Olivier Mondain-Monval, Olivier Poncelet and Christophe Aristégui, **Applied Physics Letters** **101**, 011913 (2012)

"Impact of polydispersity on multipolar resonant scattering in emulsions", Benoit Mascaro, Thomas Brunet, Olivier Poncelet, Christophe Aristégui, Simon Raffy, Olivier Mondain-Monval, Jacques Leng, **Journal of The Acoustical Society of America** **133** (4), 1996 (2013)

"Soft acoustic Metamaterials", Thomas Brunet, Jacques Leng, Olivier Mondain-Monval, **Science** **342**, 323 (2013)

"Tuning Mie scattering resonances in soft materials with magnetic fields", Thomas Brunet, Kevin Zimny, Benoit Mascaro, Olivier Sandre, Olivier Poncelet, Christophe Aristégui, Olivier Mondain-Monval, **Physical Review Letters** **111**, 264301 (2013)

"Design of a fluorinated magneto-responsive material with tunable acoustic properties", Kevin Zimny, Benoit Mascaro, Thomas Brunet, Olivier Poncelet, Christophe Aristégui, Jacques Leng, Olivier Sandre, and Olivier Mondain-Monval, **Journal of Materials Chemistry B** **2**, 1285 (2014)